PIONEER
ACADEMIC PUBLISHING LIMITED

Current Research in Medical Sciences
ISSN 2958-0390
www.pioneerpublisher.com/crms
Volume 1 Number 1 December 2022

CSF Dynamics: Implications for Hydrocephalus and Glymphatic Clearance

Ashley Bissenas[1], Chance Fleeting[1], Drashti Patel[1], Raja Al-Bahou[1], Aashay Patel[1], Andrew Nguyen[1], Maxwell Woolridge[1], Conner Angelle[1] & Brandon Lucke-Wold[1]

[1] Department of Neurosurgery, University of Florida, Gainesville, Florida, USA
Correspondence: Brandon Lucke-Wold, Department of Neurosurgery, University of Florida, Gainesville, Florida, USA.

doi:10.56397/CRMS.2022.12.04

Abstract

Beyond its neuroprotective role, CSF functions to rid the brain of toxic waste products through glymphatic clearance. Disturbances in the circulation of CSF and glymphatic exchange are common among those experiencing HCP syndrome, which often results from SAH. Normally, the secretion of CSF follows a two-step process, including filtration of plasma followed by the introduction of ions, bicarbonate, and water. Arachnoid granulations are the main site of CSF absorption, although there are other influencing factors that affect this process.

The pathway through which CSF is through to flow is from its site of secretion, at the choroid plexus, to its site of absorption. However, the CSF flow dynamics are influenced by the cardiovascular system and interactions between CSF and CNS anatomy. One, two, and three-dimensional models are currently methods researchers use to predict and describe CSF flow, both under normal and pathological conditions. They are, however, not without their limitations. "Rest-of-body" models, which consider whole-body compartments, may be more effective for understanding the disruption to CSF flow due to hemorrhages and hydrocephalus.

Specifically, SAH is thought to prevent CSF flow into the basal cistern and paravascular spaces. It is also more subject to backflow, caused by the presence of coagulation cascade products. In regard to the fluid dynamics of CSF, scar tissue, red blood cells, and protein content resulting from SAH may contribute to increased viscosity, decreased vessel diameter, and increased vessel resistance. Outside of its direct influence on CSF flow, SAH may result in one or both forms of hydrocephalus, including noncommunicating (obstructive) and communicating (nonobstructive) HCP.

Imaging modalities such as PC-MRI, Time-SLIP, and CFD model, a mathematical model relying on PC-MRI data, are commonly used to better understand CSF flow. While PC-MRI utilizes phase shift data to ultimately determine CSF speed and flow, Time-SLIP compares signals generated by CSF to background signals to characterizes complex fluid dynamics.

Currently, there are gaps in sufficient CSF flow models and imaging modalities. A prospective area of study includes generation of models that consider "rest-of-body" compartments and elements like arterial

pulse waves, respiratory waves, posture, and jugular venous posture. Going forward, imaging modalities should work to focus more on patients in nature in order to appropriately assess how CSF flow is disrupted in SAH and HCP.

Keywords: cerebrospinal fluid, glymphatic system, subarachnoid hemorrhage, communicating hydrocephalus, noncommunicating hydrocephalus

1. Introduction

1.1 The Role of Cerebrospinal Fluid

Cerebrospinal fluid (CSF) is a clear fluid produced by ependymal cells that line the choroid plexus of the brain's ventricular system; this fluid bathes not only the brain but the spinal cord as well, with CSF running throughout the entirety of the subarachnoid spaces (SAS) of the central nervous system (Ma Q, Schlegel F, Bachmann SB, et al, 2019). CSF is thought to primarily act to protect the brain from blunt-force trauma and coup-contrecoup injuries by cushioning the blow between the cranium and brain parenchyma (Andersson K, Manchester IR, Andersson N, Shiriaev A, Malm J & Eklund A., 2007). However, more recent research continues to expand upon not only understanding the creation and elimination of CSF, but also the possibility of its other vital functions. In regard to origin and composition, while the primary mode of CSF production arises from ependymal cells, there is also transport of fluid and macromolecules from capillary and choroid plexus interstitial space into CSF (Jessen NA, Munk ASF, Lundgaard I & Nedergaard M., 2015). Although such transport is limited by tight junctions between choroid plexus epithelial cells, such provides a previously undiscovered mediator of CSF ion and macromolecule concentration. Similarly, within the last decade, the discovery of meningeal lymphatics within dural sinuses that can carry CSF in perivenous down to cervical lymph nodes challenged the notion that absorption through arachnoid villi was the only method of filtration or elimination of waste products from CSF (Louveau A, Smirnov I, Keyes TJ, et al., 2016; Eklund A, Smielewski P, Chambers I, et al., 2007). This knowledge also supports the notion that CSF acts as more than just a cushion for the brain. It also functions to clear waste products from brain parenchyma (Kaur J, Fahmy LM, Davoodi-Bojd E, et al., 2021). Knowing such, there are still many questions regarding the specifics of CSF dynamics and so-called "glymphatic clearance", especially in determining the relative importance of interstitial fluid in perivascular spaces and the separate SAS through which CSF runs through (Daversin-Catty C, Vinje V, Mardal KA & Rognes ME, 2020). Still, these new findings can hold promise in elucidating mechanisms and potential therapeutic targets for conditions such as neurodegenerative diseases, hydrocephalus (HCP), and subarachnoid hemorrhage (SAH).

1.2 Subarachnoid Hemorrhages, Hydrocephalus, and the Glymphatic System

The incidence of acute SAH is approximately 2 to 22 individuals per 100,000 every year (Feigin VL, Lawes CM, Bennett DA, Barker-Collo SL & Parag V., 2009). Of those, 85% are said to be caused by a rupture in an aneurysm, often found within a basal cerebral artery (Kundra S, Mahendru V, Gupta V & Choudhary A., 2014). The mortality of aneurysmal SAH is estimated at 30% (Petridis AK, Kamp MA, Cornelius JF, et al., 2017). Risk factors associated with SAH include cardiovascular risk factors such as hypertension, hypercholesterolemia, smoking, and excess alcohol intake (Feigin VL, Rinkel GJE, Lawes CMM, et al., 2005). At present, computed tomography is the preferred imaging method for diagnosing subarachnoid bleeding (Petridis AK, Kamp MA, Cornelius JF, et al., 2017).

One of the most common complications of acute SAH is acute (0-3 days post-SAH), subacute (4-13 days), or chronic (14+ days) HCP (Kwon JH, Sung SK, Song YJ, Choi HJ, Huh JT & Kim HD., 2008). HCP is characterized by enlargement of the temporal horns of the lateral ventricles (Kwon JH, Sung SK, Song YJ, Choi HJ, Huh JT & Kim HD., 2008). There are two main combinations of HCP

invoked from SAH, communicating (nonobstructive) and noncommunicating (obstructive) (Hartman A., 2009; Bhattacharjee S, Rakesh D, Ramnadha R & Manas P., 2021). Communicating HCP occurs when CSF is blocked after exiting ventricles; however, CSF can still disperse between ventricles. One form of communicating HCP, normal pressure HCP (NPH), is commonly found in those 50 years and older and occurs in response to a gradual blocking of CSF drainage over time (M Das J & Biagioni MC., 2022). In NPH, there is a high-normal CSF pressure imbalance in CSF absorption and production (Brust JCM., 2019). Communicating HCP can also be caused by impaired absorption of CSF at the arachnoid granulations (Koleva M & De Jesus O., 2022). In contrast, noncommunicating HCP results from obstruction of the CSF flow pathway (Koleva M & De Jesus O., 2022). In the case of SAH, chronic HCP is often of the communicating type, resulting from scar tissue blockage of arachnoid granulation (Chen S, Luo J, Reis C, Manaenko A & Zhang J., 2017), while acute HCP results from blood clots within the ventricles and cerebral aqueduct (noncommunicating HCP) (Chen S, Luo J, Reis C, Manaenko A & Zhang J., 2017).

In blocking CSF absorption at the arachnoid granulations post-SAH, glymphatic clearance of CSF and its critical role in SAH must be considered (Fang Y, Huang L, Wang X, et al., 2022). During SAH, blood not only enters the SAS to mix with CSF, but it can also create an intraventricular hemorrhage (IVH) by directly interacting with CSF at the site of synthesis. When considering the potential for blood to hold toxic metabolites from damaged brain parenchyma, clearance of this metabolite-containing blood becomes even more critical. However, because SAH causes blood to rush into perivascular spaces (Galli F, Pandolfi M, Liguori A, Gurgitano M & Sberna M., 2021), the regular flow and communication of CSF and interstitial fluid may be disrupted. Thus, glymphatic clearance can be diminished (Quintin S, Barpujari A, Mehkri Y, Hernandez J & Lucke-Wold B., 2022). Similarly, the advanced age of those typically experiencing SAH can also play a deleterious role in preventing recovery, with pre-clinical evidence showing decreased glymphatic clearance in aged rats (Li L, Ding G, Zhang L, et al., 2022). A decrease in glymphatic flow with heightened age and SAH creates a deadly combination, with such potentially leading to increased intracranial pressure (ICP) and enlarged ventricles characteristic of HCP.

In all cases of HCP, the pulse dynamics and flow of CSF are altered, and ICP is increased. Under normal conditions, CSF circulates continuously with a balance between the rate of production and the rate of storage and reabsorption (Papaioannou V, Czosnyka Z & Czosnyka M., 2022). The circulatory flow results from hydrostatic pressure gradients, causing CSF secretion by the choroid plexuses and resorption at the arachnoid granulations (Whedon JM & Glassey D., 2009). However, CSF also circulates in pulses due to compression of the brain ventricles by systolic arterial expansion, resulting in CSF movement into the SAS (Whedon JM & Glassey D., 2009).

2. Cerebrospinal Fluid Under Nonpathological Conditions

2.1 Cerebrospinal Fluid Secretion and Absorption

The first step in normal physiological CSF flow is CSF secretion, which is a two-step process in itself (Sakka L, Coll G & Chazal J., 2011). The main method of secretion occurs at the choroid plexus, which consists of granular meningeal protrusions into the ventricular lumen (Speake T, Whitwell C, Kajita H, Majid A & Brown PD., 2001). The cells of the choroid plexus also contain microvilli at their apical surface and are interconnected by tight junctions (Maria João Manzano, 2004). The first step in CSF secretion consists of passive filtration of plasma as it moves from the choroidal capillaries to the choroidal interstitial compartment, powered by a pressure gradient (Brinker T, Stopa E, Morrison J & Klinge P., 2014). This is then followed by transport of plasma from the interstitial compartment to the ventricular lumen across the choroidal epithelium. This second step is accompanied by the formation of bicarbonate and other ions from enzymes that are pumped into the ventricular lumen. Water subsequently follows this ion gradient (Owler BK, Pitham T & Wang D., 2010; Damkier HH, Brown PD & Praetorius J., 2013). Regulation of CSF secretion occurs through the NaK2Cl cotransporter on the apical membrane (Gregoriades JMC, Madaris A, Alvarez FJ &

Alvarez-Leefmans FJ., 2019). This transporter works bi-directionally and can upregulate or downregulate CSF based on physiological needs (Sakka L, Coll G & Chazal J., 2011). The choroid plexus is responsible for the majority of CSF secretion, while a minor amount is contributed by extra chorial secretion such as the ependymal wall, cerebral parenchyma, and interstitial fluid (Khasawneh A, Garling R & Harris C., 2018).

CSF secretion is not continuous and is instead finely regulated. An increase in intraventricular pressure will cause a decrease in the pressure gradient across the blood-brain barrier, decreasing plasma filtration and thus CSF secretion. Beyond pressure, the choroid plexus is under the influence of the cholinergic, adrenergic, serotonergic, and peptidergic autonomic aspects of the sympathetic nervous system. Sympathetic nervous system activity decreases the secretion of CSF, while parasympathetic nervous system activity inversely increases secretion (Sakka L, Coll G & Chazal J., 2011). The autonomic nervous system is also aided by monoamines and neuropeptide factors that influence the secretion of CSF. Dopamine, serotonin, melatonin, Atrial Natriuretic Peptide (ANP) and Arginine Vasopressin (AVP) receptors are present on the surface of the choroidal epithelium, with activation of the latter two decreasing CSF secretion (Faraci FM, Mayhan WG & Heistad DD., 1990). The availability of these receptors for their corresponding peptides varies among individuals, which may account for differences in CSF secretion. Variation in receptor expression has also been linked to certain pathologies, including HCP.

Circulation of CSF is dynamic in the human system, and cerebral homeostasis is maintained by the regulation of CSF circulation. CSF flows from the site of secretion toward the site of absorption. CSF produced by the choroid plexuses in the lateral ventricles travels through interventricular foramina to the third ventricle, to the fourth ventricle via the cerebral aqueduct, and finally to the SAS via the median aperture of the fourth ventricle (Khasawneh A, Garling R & Harris C., 2018). Within the cerebral SAS, CSF flows either toward the site of absorption or to the spinal SAS (Kartalcı Ş, Erbay MF, Kahraman A, Çandır F & Erbay LG., 2021).

After circulating, the main route of CSF absorption is via the cranial arachnoid granulations (Spector R, Robert Snodgrass S & Johanson CE., 2015). Arachnoid villi extend from the dura mater into the venous sinuses, creating spaces for CSF absorption (Welch K & Friedman V., 1960). Like CSF secretion, a pressure gradient between the SAS and the venous sinuses is important in the drainage of CSF into the sinuses (Pollay M., 2010). It has been shown experimentally that modulations in the SAS pressure allow for reabsorption, as the pressure in the superior sagittal sinus remains constant relative to fluctuations in CSF pressure (Davson H, Hollingsworth G & Segal MB., 1970). Within the SAS, there are variations in the arachnoid space meningeal sheath that allow for CSF reabsorption independent of variations in anatomical features. Some villi partially cross while others completely cross the dural membranes with various surface areas of exchange according to the degree of application of the arachnoid layer (Sakka L & Coll G, Chazal J., 2011). Absorption of CSF by the arachnoid processes is not static and can adapt to variations in pressure to maintain constant cerebral pressure, thus avoiding injury.

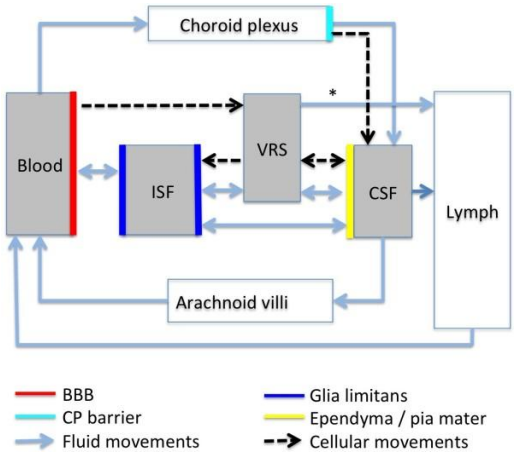

Figure 1. Normal CSF Circulation

CSF circulates across different compartments and through many barriers, including the blood-brain barrier. Osmotic and hydrostatic pressure gradients are responsible for the exchange of CSF across compartments, along with active transport across glial cells, endothelial cells, and choroid plexus. This figure highlights the only direct connection between blood plasma and CSF, which is found at the main site of CSF secretion, choroid

plexus of the ventricles. (Brinker T, Stopa E, Morrison J & Klinge P., 2014)

2.2 Cerebrospinal Fluid Dynamics in Subarachnoid Space

CSF flow within the SAS is an important part of the brain's waste-clearing system. Currently, there are many theories on normal fluid dynamics within the brain that aid in the clearance of CSF and other metabolites. Within the SAS, CSF flow was previously thought to have been either down through the spinal cord or up over the cerebral convexities before being absorbed in the arachnoid granulations and arachnoid villi (Bradley WG., 2015). Recent studies have challenged this view. The perivascular flow model describes CSF flow in the SAS similar to lymphatic flow in the rest of the body. This glymphatic theory of flow describes the route of CSF in the SAS as an influx of CSF in periarterial spaces, convective flow through the interstitium, followed by efflux into perivenous spaces (Daversin-Catty C, Vinje V, Mardal KA & Rognes ME., 2020). Further supporting evidence comes from the use of MRI imaging in mice models, which has demonstrated this route of CSF flow (Iliff JJ, Lee H, Yu M, et al., 2013).

Within the SAS, the flow of CSF is not static nor steady but is subject to a complex pulsating motion that is in sync with the heartbeat (Donatelli D & Romagnoli L., 2020). Further complicating the flow of CSF is its movement within the spinal cord SAS, specifically below the level of S2 where CSF encounters spinal cord and dorsal and ventral nerve rootlets. Current mathematical models that have attempted to characterize normal fluid dynamics in healthy patients as a synchronized, pulsating relationship between CSF and the cardiovascular system include one-dimensional flexible coaxial pipe models (Martin BA, Reymond P, Novy J, Balédent O & Stergiopulos N., 2012; Cirovic S & Kim M., 2012), two-dimensional axisymmetric models (Bertram CD, Brodbelt AR & Stoodley MA., 2005), and three-dimensional models that include fluid-structures (Clarke EC, Fletcher DF, Stoodley MA, Bilston LE, 2013).

Each of these computational models provides its strengths and limitations. For example, one-dimensional coaxial pipe models, which simplify vasculature to straight segments, were remarkably capable of capturing similar waveform properties of CSF dynamics as measured *in vivo*, such as a rhythmic delay in peaks of CSF flow following peaks of cerebral blood flow and a similar attenuation of the CSF flow waveform in the spinal SAS following increased compliance, corroborating MRI measurements in healthy patients (Martin BA, Reymond P, Novy J, Balédent O & Stergiopulos N., 2012). Another one-dimensional model captured similar *in vivo* wave-propagation properties throughout the CSF compartment in the presence of various pressure disturbances, demonstrating a mathematical relation between the elasticities of different spinal cord membranes and CSF propagation (Cirovic S & Kim M., 2012). Due to their simplicity, one-dimensional models provide the added benefit of reduced computational costs and simpler numerical methods, enabling ease of results interpretation. However, due to assumptions and the failure to account for the presence of anatomical structures like nerve roots and arachnoid trabeculae that may produce secondary flow obstructions and wall shear stress, the results produced from these models may be altered (Martin BA, Reymond P, Novy J, Balédent O & Stergiopulos N., 2012).

The two-dimensional model builds upon the one-dimension model's assumptions by utilizing axisymmetric representations of the spinal cord in approximating the spinal cord's anatomy using progressively tapered segments cranially to caudally (Bertram CD, Brodbelt AR & Stoodley MA., 2005). With this increased-complexity model, it was demonstrated that the CSF waveform properties vary depending on the compressibility of the composition of the spinal cord itself, as well as the elasticity of surrounding structures, including the dura mater, fat, and vertebral bone. Additionally, this model highlights that there are no waveform changes when the central spinal canal is present or absent, indicating its lack of a role in CSF flow wave propagation (Bertram CD, Brodbelt AR & Stoodley MA., 2005). Finally, most closely mirroring actual human anatomy, is the three-dimension model, which represents the SAS in volumetric space, largely determined by MRI measurements. Due to its comprehensiveness and consideration of the effect of trabecular structures on CSF flow, this model is capable of capturing the

more complicated picture of CSF dynamics as it is impacted by compressions of blood vessels and movements of the ventricular walls (Clarke EC, Fletcher DF, Stoodley MA & Bilston LE., 2013). However, two- and three-dimensional models are limited in practice due to their computational complexity and complicated underlying numerical assumptions, such as multi-dimensional Navier-Stokes equations to describe vessel wall displacements and physiological fluid dynamics (Bertram CD, Brodbelt AR & Stoodley MA., 2005; Clarke EC, Fletcher DF, Stoodley MA & Bilston LE., 2013; Formaggia L, Gerbeau JF, Nobile F & Quarteroni A., 2001; Del Bigio MR., 2001).

The aforementioned models share assumptions regarding the compartmentalization of CSF. To simplify calculations and better contextualize the involved anatomical structures and related CSF dynamics, these models rely on a lumped-compartment system where parameters such as pressure, volume, and flow changes are dependent on parameters contained in adjacent compartments (Martin BA, Reymond P, Novy J, Balédent O & Stergiopulos N., 2012; Cirovic S & Kim M., 2012; Bertram CD, Brodbelt AR & Stoodley MA., 2005; Clarke EC, Fletcher DF, Stoodley MA & Bilston LE., 2013). However, recently there have been challenges to the lumped-compartment system, as it assumes that CSF flow is a closed-looped system with constant total volume due to equal inflow to outflow. This assumption fails to capture extracranial influences on CSF flow, as is thought to occur with pathophysiology. Recent computational models have moved beyond this assumption by incorporating "rest-of-body" compartments, including lymphatic vessels, cardiac ventricles, and peripheral vasculature (Van De Vyver AJ, Walz AC, Heins MS, et al., 2022). This new approach allows for the study of CSF dynamics in the context of different bodily functions, such as sympathetic and parasympathetic autoregulation, central body fluid ingestion and excretion, and peripheral cardiovascular phenomena, such as cardiac arrest or hemorrhages (Lakin WD, Stevens SA, Tranmer BI & Penar PL., 2003).

Both reduced models and more sophisticated ones have proven useful in describing the fluid dynamics of CSF. Reduced models adequately represent the global behavior of the physiological circulatory system, while advanced models better describe more localized phenomena that interact with a larger global model. However, other factors aside from interactions with microanatomy affect the normal flow of CSF in the SAS, including arterial pulse waves, respiratory waves, posture, and jugular venous posture (Sakka L, Coll G & Chazal J., 2011).

3. Cerebrospinal Fluid Under Pathological Conditions

3.1 Pathophysiology and Disruption of Circulation and Dynamics in Subarachnoid Hemorrhage

CSF dynamics and circulation is a particularly vital element in the context of SAH and its ensuing sequelae. The aforementioned sequelae of SAH regarding CSF can be succinctly described as such:

1) SAH is ensued by bleeding into the SAS

2) Erythrocyte coagulative products from lytic events accumulate in the SAS

3) Acute vasoconstriction termed vasospasm occurs

4) CSF flow is impaired, carrying over important consequences for its role in glymphatic clearance (Loftspring MC, Wurster WL, Pyne-Geithman GJ & Clark JF., 2007; Zhou J, Guo P, Guo Z, Sun X, Chen Y & Feng H., 2022).

Preclinical studies—namely, animal models and computational analyses have elucidated a potential role for pathological CSF flow in promoting the morbid consequences of SAH, including vasospasm coagulation, increased ICP, and delayed ischemia (Wang HB, Wu QJ, Zhao SJ, et al., 2020).

Several in vitro and animal models from 2014 to 2017 have provided further insight into SAH and its influence on the physiological flow of CSF. In a study of CSF dynamics in a mice model by Siler et al., experimental SAH was introduced via perforation of the circle of Willis. Subsequent CSF flow was assessed following injection of fluorescent tracers into the cisterna magna 1 hour following SAH. Several key observations were made among SAH-induced subjects. Firstly, compared to control mice, CSF is unable to flow into the basal cistern and paravascular spaces. Secondly, immunofluorescent staining of

fibrinogen in the paravascular spaces is markedly increased. This suggests a backflow of CSF caused by fibrinogen deposits as a result of blood invasion into the SAS and paravascular region (Siler DA, Gonzalez JA, Wang RK, Cetas JS & Alkayed NJ., 2014). Further enhancing these observations, intracisternal injection of tPA in three groups (control, SAH + CSF, SAH + tPA) revealed a restoration of CSF distribution in SAH mice treated with tPA, particularly in the basal cistern and paravascular routes.

These findings were supplemented by Golonav et al. in a similar analysis of a SAH-induced mouse nervous system. Their fluoroscopic experiments displayed an accumulation of blood also in the basal cisterns and perivascular space, with a restriction of CSF flow beyond the frontal areas of the basal regions. Likewise, increased fibrin presence paralleled the areas of blood invasion in SAH mice, with cascade inhibition (tissue factor [TF] antibody) restoring CSF distribution compared to controls (Golanov EV, Bovshik EI, Wong KK, et al., 2018; Gaberel T, Gakuba C, Goulay R, et al., 2014; Wang KC, Tang SC, Lee JE, et al., 2018). Collectively, these results allude to the importance of the coagulation cascade in impaired CSF dynamics following SAH (Goulay R, Flament J, Gauberti M, et al., 2017). Though initial bleeding may impair flow, it is the eventual fibrin and fibrinogen degradation products that block CSF flow conducive to vasospasm, ultimately manifesting as increased ICP and delayed ischemia. Though, perhaps not pathognomic, perse, the presence of these products in light of prior SAH should increase suspicion for progression into delayed ischemia. Furthermore, this carries significant implications for the integrity of the glymphatic system, which is primarily facilitated by CSF. While not directly pertinent to the clinical sequence towards ischemia, an impairment of crucial waste clearance and nutrient distribution agents is worth nothing (Gaberel T, Gakuba C, Goulay R, et al., 2014; Plog BA & Nedergaard M., 2018).

3.2 Other Biomarkers and Analyses of Cerebrospinal Fluid Dynamics

Other in-vitro studies have also explored CSF interactions in the setting of SAH. Namely, Loftspring et al.'s assessment of the role of bilirubin and its oxidation products in CSF as a cause of vasospasm in rats (Loftspring MC, Wurster WL, Pyne-Geithman GJ & Clark JF., 2007). High-performance liquid chromatography revealed elevations in BOXes and coincided with other elevated measures of oxidative stress (MDA) within the CSF. This experiment did not analyze flow parameters directly, yet it suggests another potential cause for impaired CSF flow in SAH-afflicted patients.

Various studies have, however, assessed the physical mechanisms of effective SA blood clearance as a means to mitigate the progression toward vasospasm. Kertzscher et al. postulated that hypoperfusion of CSF following SAH is an important driver of vasospasm and ischemia as a result of decreased blood clearance (Kertzscher U, Schneider T, Goubergrits L, Affeld K, Hänggi D & Spuler A., 2012). Therefore, the role of CSF circulation, or lack thereof, in the downstream effects of SAH is highlighted. They describe a two-stage mechanism in which blood and CSF mix and subsequently clear together via the mode of CSF flow, and, more applicably, how this can be utilized in the event of SAH. Importantly, specific events such as effective mixing preclude blood clearance, as the viscosity of the blood and CSF discourage sufficient mixing without thorough shaking. To corroborate this, a 3D silicone model of the human basal cistern was constructed from MRI data for physical simulation. Blood clearance was found to increase with two specific parameters in head shaking, higher shaking angles and slower head shaking frequencies. The importance of the shaking angle is driven by the dependence of such mixing on the natural alignment of the earth's gravitational force. Aligning the angle of shaking so that both CSF and blood regions are optimally layered and enacted on by this force maximizes the degree of mixing. Regarding the shaking frequency, low blood viscosity necessitates lower shaking frequencies to ensure ample duration in the fluid mixture. Other explicit parameters of CSF dynamics have been studied in clinical subjects (Kazumata K, Kamiyama H, Ishikawa T, et al. 2006; Kosteljanetz M., 1984).

3.3 Mechanism and Model of Cerebrospinal Fluid Flow Changes Due to Subarachnoid Hemorrhage

The main physical perturbations assumed through the mechanism of injury of a SAH are a change in

fluid viscosity due to the increased presence of blood cells and proteins and the formation of obstructions and constrictions via scar tissue formation. Following the classical multicompartmental model of CSF hemodynamics (Lakin WD, Stevens SA, Tranmer BI & Penar PL., 2003; Ursino M & Lodi CA., 1997), both the increased viscosity (η) and the constriction of the vessel radius (r) cause an increase in the vessel resistance (R) locally to the injury as well as near bottle-neck points or chokes, such as the cerebral aqueduct. Through Poiseuille's Law, the direct individual effect of each of these perturbations on the volumetric flow rate is expressed through the following partial derivatives (Ursino M & Lodi CA., 1997):

$$\frac{\partial R}{\partial \eta} = \frac{8L}{\pi r^4}$$
$$\frac{\partial R}{\partial r} = \frac{-32L\eta}{\pi r^5}$$

Additionally, increasing the viscosity, increasing the density, and constricting the vessel diameter may contribute to an increase in the turbulence; however, at physiological flow rates of CSF, it is unlikely that this would cause any significant turbulent flow outside of the standard locations that would otherwise be observed (Bertram CD, Brodbelt AR & Stoodley MA., 2005; Shinya Yamada, 2021). In either case, both the viscosity and constricted diameter could have the potential to increase shear damage and pathological pressure differentials, leading to localized damage within the SAS (Jacobson EE, Fletcher DF, Morgan MK & Johnston IH., 1999). In perpetuating the intravascular damage and possibly causing systemic capacitive effects in the intracranial circulatory system and brain, a secondary injury may result.

It should be noted that empirical studies have found that the increased cellular and protein content in SAS post-hemorrhage likely has little effect on the bulk viscosity of the CSF at the physiological flow rates and concentrations (Bloomfield IG, Johnston IH & Bilston LE., 1998). This does not necessarily discount local effects but does imply the absence of global physical effects due to the diffusion of humeral contents. Furthermore, individual aqueductal CSF hydrodynamics vary significantly in both magnitude and direction following a cranial SAH, implying that any standard tractable effect may be overshadowed (Lindstrøm EK, Ringstad G, Sorteberg A, Sorteberg W, Mardal KA & Eide PK., 2019). This may be due to the fact that purely fluid-dynamic models fail to account for spasmogen interactions and active compensation.

In a similar vein, Abolfazli et al. developed an MRI-based finite element model to track CSF dynamics following SAH to assess the efficacy of lumbar drainage (Abolfazli E, Fatouraee N & Seddighi AS., 2016). In this model, the acute effect of subarachnoid hemorrhaging was modeled as 20 ml of blood being released into the SAS. Lumbar drainage was found to effectively accelerate the clearance of blood and related spasmogens proportional to the rate of drainage. This has since been corroborated by computational fluid dynamic modeling (Khani M, Sass LR, Sharp MK, et al., 2020). This style of modeling is growing in popularity as MRI imaging advances, allowing for finite element simulations to be built at a patient-specific level (Li X., 2021; Wittek A, Joldes G, Couton M, Warfield SK & Miller K., 2010; Lefever JA, Jaime García J & Smith JH., 2013). Coupling this style of simulation with pathological perturbations could expose prognostic markers and help physicians efficiently create patient treatment plans at an individual level.

3.4 Pathophysiology and Disruption of Circulation and Dynamics in Obstructive, Nonobstructive, and Normal Pressure Hydrocephalus

Another effect of abnormal CSF distribution is HCP, which is caused by an imbalance in the production and circulation of CSF. Typically, CSF production and reabsorption are equal, and the homeostatic range for ICP lies between 600-2000 Pa (Vardakis JC, Tully BJ & Ventikos Y., 2013). When more CSF is produced than reabsorbed, it accumulates in the ventricular cavities of the brain, increasing the ICP above 2000 Pa, which can lead to brain damage or pressure-induced atrophy in patients (Gholampour S & Fatouraee N., 2021). The long-term implications of HCP range from dementia and impaired myelin production (Del Bigio MR., 2001) to metabolic acidosis and peritonitis in the abdomen. The causes of HCP come from a wide variety of genetic or acquired disorders. The abnormal proliferation of glial cells, known as gliosis, can lead to HCP (Balestrazzi P,

de Gressi S, Donadio A & Lenzini S., 1989). Inflammation or scarring of the arachnoid mater is also another potential cause of HCP (Koleva M & De Jesus O., 2022). The disruption of CSF dynamics can ultimately lead to two types of HCP: noncommunicating (obstructive) hydrocephalus and communicating (nonobstructive), which includes the subtype of normal pressure.

Noncommunicating HCP blocks communication between the ventricles of the brain, and it is also referred to as venous congestive HCP due to the compression of superficial veins in the cerebral hemispheres as a result of ventricular dilation from CSF buildup (Greitz D, Greitz T & Hindmarsh T., 1997). The most common sites of obstruction occur proximally to granulations, including in the interventricular foramen, cerebral aqueduct, fourth ventricle, and foramen magnum (Sokal P, Birski M, Rusinek M, Paczkowski D, Zieliński P, Harat A., 2012). Brain tumors of significant size can also obstruct CSF pathways. For instance, pineal gland tumors are frequently responsible for causing aqueductal stenosis, and colloid cysts can obstruct the interventricular foramen (Figure 2). Other tumors that impede CSF flow include hypothalamic and optic nerve glia, choroid plexus papilloma, craniopharyngioma, pituitary adenoma, posterior fossa tumors, and metastatic tumors. Once noncommunicating HCP is diagnosed, the primary goal is to locate the obstacle blocking CSF for safe removal (Farb R & Rovira À., 2020). If the obstruction cannot be removed, then the path of CSF must be diverged to reduce the patient's ICP.

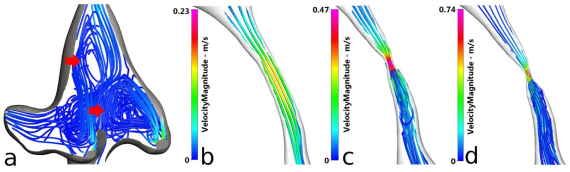

Figure 2. CSF Velocities in Cerebral Aqueduct Stenosis

CSF flows in many directions at different speeds in the cerebral aqueduct and 4th ventricle (*a*). In a healthy subject (*b*), CSF velocity through the cerebral aqueduct is normal. In a mildly stenosed patient (*c*), CSF velocity decreases significantly below the obstruction. In a severely stenosed patient (*d*), CSF velocity is hazardously low below the obstruction, and the ventricle is enlarged. In addition, areas of dead zones were noticed in the lateral ventricles of the patient (*d*) after the velocities were calculated (Vardakis JC, Tully BJ & Ventikos Y., 2013).

Communicating HCP is also known as nonobstructive because the flow of CSF through the ventricular system is not blocked (Koleva M & De Jesus O., 2022). Communicating HCP may result from an occlusion or lesion that prevents the flow of CSF within the ventricular system (Vardakis JC, Tully BJ & Ventikos Y., 2013); however, it can also be caused by impaired CSF reabsorption. Similar to noncommunicating HCP, there are many potential complex causes, such as hemorrhage, bacterial meningitis, leptomeningeal carcinomas, vestibular schwannomas, and head trauma (Maller VV, Gray RI., 2016). SAH accounts for approximately one-third of these cases, as it impairs the arachnoid granulations that typically absorb CSF, making it the most common cause of communicating HCP. Communicating HCP typically results in restricted arterial pulsations, which is why it is also referred to as restricted arterial pulsation HCP (Greitz D, Greitz T & Hindmarsh T., 1997). In communicating HCP, CSF flow through the foramen magnum is predominantly blocked, which can lead to long-term damage to nerves, cardiovascular issues, and mental impairment. Additionally, communicating HCP is often a consequence of noncommunicating HCP and the factors that caused it (Farb R & Rovira À., 2020). Treatment for communicating HCP ranges widely depending on the underlying causes.

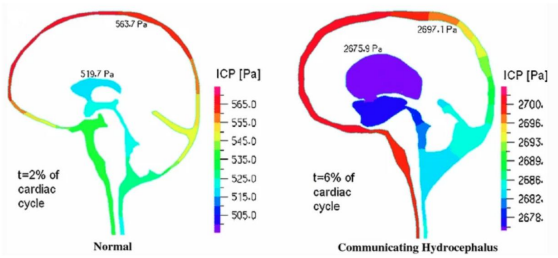

Figure 3. ICP Dynamics Between a Normal Subject and a Hydrocephalic Patient

This figure shows a simulation of ICP dynamics between a normal subject (*left*) and a patient with communicating HCP (*right*). The ICP of the

normal subject stays between 500-600 Pa, but the ICP of the patient with HCP increases to 2600-2700 Pa. Further, the stimulation shows an enlargement of the ventricles, conveying the extent to which HCP can compress the vasculature in the brain (Linninger AA, Sweetman B & Penn R., 2009).

Normal pressure hydrocephalus (NPH), a type of communicating HCP, is rare and typically does not present until after 70 years of age; furthermore, about half of these cases are idiopathic (iNPH) (Farb R & Rovira À., 2020). In NPH, ICP is typically within a normal homeostatic range. NPH has impaired circulation of CSF, and the pathophysiology is not well understood. Hypertension and white matter disease are both contributing factors for NPH (Krauss JK, Regel JP, Vach W, Droste DW, Borremans JJ & Mergner T., 1996; Tang Y min, Yao Y, Xu S, et al., 2021). The primary treatment for NPH is diverting CSF promptly using a shunt, particularly if the patient is at risk for dementia (Vivas-Buitrago T, Lokossou A, Jusué-Torres I, et al., 2019).

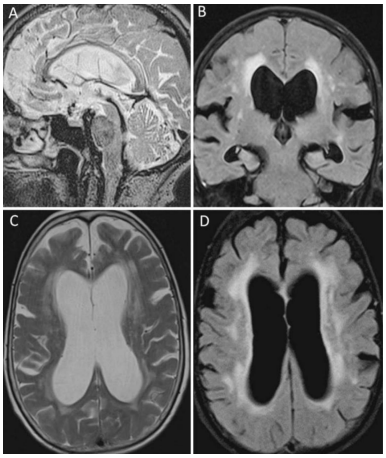

Figure 4. Radiological Features of iNPH

A 78-year-old woman with a one-year history of gait disturbances, cognitive impairment, and urinary incontinence presents with an enlarged interventricular foramen (*A*), ventriculomegaly (*B*), and sulcal dilation changes with an enlarged subarachnoid space (*C, D*) (Farb R, Rovira À., 2020).

Overall, HCP has many complex congenital and environmental causes. There is no known cure, and current treatment methods have very high rates of failure. Shunt implants are expensive, often unsuccessful, and frequently lead to other detrimental complications. Other surgical interventions, such as endoscopic third ventriculostomy, lack well-researched information about long-term success or survival rates (Vardakis JC, Tully BJ & Ventikos Y., 2013). The discovery of alternative methods to treat HCP is an ongoing area of study, requiring further research and attention.

4. Competing Imaging Modalities

Given the essential physiological role of the CSF in CNS health and its implication in neuropathologies such as HCP, it is vital to obtain a deeper understanding of CSF fluid dynamics. Many advanced imaging modalities have been developed to further study CSF fluid volume, flow, and circulation in humans to better understand its implication in health and disease. Among the most commonly used imaging modalities for the assessment of CSF fluid dynamics is phase-contrast magnetic resonance imaging (PC-MRI) (Korbecki A, Zimny A, Podgórski P, Sąsiadek M & Bladowska J., 2019). PC-MRI is a non-invasive imaging technique used to visualize and quantify moving fluids like CSF without the need for a tracer (Yamada S & Kelly E., 2016), making it the preferred method for studying real-time fluid dynamics in sensitive systems like the CNS. Like all MRI modalities, PC-MRI uses phase data, which is an intrinsic property of all nuclear magnetic resonance signals. A bipolar gradient is used to calculate the degree of phase shift that moving protons exhibit, which is directly proportional to their velocity, compared to stationary protons that experience no phase shift (Wymer DT, Patel KP, Burke WF & Bhatia VK., 2020). Thus, this imaging technique helps shed light on the complex fluid dynamics of CSF by generating real-time functional data on the speed and flow of CSF.

For PC-MRI to be diagnostically useful in understanding CSF fluid dynamics, the selection of the right imaging plane becomes crucial for accurate measurements of speed and maximization of signal-to-noise ratio (Wymer DT, Patel KP, Burke WF & Bhatia VK., 2020). Specifically, the quantification of CSF flow dynamics, including mean peak velocity, can only be done in a plane perpendicular to the direction of flow (Korbecki A, Zimny A, Podgórski P, Sąsiadek M & Bladowska J., 2019). One study

found that when quantifying CSF fluid dynamics as a medical diagnostic tool, the use of cardiac-gated PC-MRI in the sagittal plane, which is flow-sensitive in the craniocaudal direction (along the readout axis), yielded a better overall assessment of CSF flow dynamics. However, the use of a cardiac-gated PC-MRI high-resolution axial technique, which is sensitive to through-plane flow, was better at measuring the rate of CSF flow through the cerebral aqueduct. In a clinical context, the use of cardiac-gated PC-MRI high-resolution axial technique was the only technique that provided accurate data for helping to distinguish between normal and abnormal CSF flow dynamics (Nitz WR, Bradley WG, Watanabe AS, et al., 1992).

The selection of the right image plane for PC-MRI is not its only limitation. For instance, the cardiac-gating of PC-MRI provides functional average data constricted to the heart cycle, which omits the complexity of CSF flow dynamics and its association with other factors like respiration and real-time multidirectional CSF flow (Korbecki A, Zimny A, Podgórski P, Sąsiadek M, Bladowska J., 2019). Recent advances in neuroimaging have sought to address this problem. The time-spatial spin labeling inversion pulse (Time-SLIP) tackles complex fluid dynamic patterns, such as the turbulent flow between the cerebral aqueduct and the third ventricle that is not detected with PC-MRI (Korbecki A, Zimny A, Podgórski P, Sąsiadek M, Bladowska J., 2019). In Time-SLIP, CSF itself acts as a contrast agent, and it is marked by radio frequency pulses. This allows for concurrent characterization of CSF fluid dynamics and suppression of the background signal with an inversion pulse (Yamada S & Kelly E., 2016). Contrasting signal differences between labeled CSF and background signal provide a useful method for assessing CSF flow at any given time (Yamada S, Tsuchiya K, Bradley WG, et al., 2015). While PC-MRI is still a leading technique that provides both qualitative and quantitative data about CSF flow dynamics, it is constrained to the cardiac cycle. Time-SLIP corrects this limitation by providing a different perspective on CSF flow dynamics, accounting for its pulsatile and bulk flow.

Another competing imaging modality that aims to study CSF flow dynamics is the computational fluid dynamics (CFD) model, a non-invasive technique that uses mathematical analysis to solve complex and intricate fluid dynamics problems. The CFD model enables in silico construction and testing of fluid dynamics that might not be easily tested in real time. This enables a better understanding of the complexity of CSF flow by controlling for different factors and allowing for the isolation of a phenomenon of interest, including CSF flow in healthy and diseased populations. The application of the CFD model in the study of CSF dynamics is based primarily on PC-MRI-generated data to reconstruct a flow model (Fillingham P, Rane Levendovszky S, Andre J, et al., 2022). While the CFD model shows potential, its dependence on MRI techniques for boundary conditions presents a problem of standardization of major parameters like the flow rate in the cerebral aqueduct. The standardization of such parameters needs to be established in order for CFD to yield relevant clinical assessments (Kurtcuoglu V., 2011). Additionally, the CFD model is limited in modeling the entirety of the CSF space, as it neglects substructures like trabeculae and transient tissue deformations (Kurtcuoglu V., 2011).

Our understanding of CSF fluid dynamics and its implication in diseases, including HCP, has been expanded due to the advancement of neuroimaging techniques. Imaging modalities like PC-MRI, MRI-based CFD models, and Time-SLIP challenge current knowledge of how CSF behaves and flows in spaces surrounding the CNS, and, by extension, our ability to accurately diagnose and treat diseases related to abnormal CSF dynamics.

Table 1. CSF Fluid Dynamics Imaging Modalities

Imaging Modality	Description	Clinical Use	Limitations	Invasive	Sample Studies
Phase-Cont	CSF fluid	Diagnosis of	Cardiac gating	No	(Battal B, Kocaoglu

rast MRI	dynamic assessment	abnormal CSF fluid flow in multiple neuropathologies (hydrocephaly, Chiari I malformations, etc)	which disregards other factors influencing CSF flow		M, Bulakbasi N, Husmen G, Tuba Sanal H, Tayfun C., 2011; Alperin N, Vikingstad EM & Gomez-Anson B, Levin DN., 1996)
Time-SLIP	CSF fluid dynamic assessment	Diagnosis of abnormal CSF fluid flow in multiple neuropathologies (hydrocephaly, Chiari I malformations, etc)	Dynamics assessment is limited to the defined labeled area using one-dimensional labeling pulse	No	(Ohtonari T, Nishihara N, Ota S & Tanaka A., 2018; Shibukawa S, Miyati T, Niwa T, et al. 2018; Takeuchi K, Ono A, Hashiguchi Y, et al., 2017; Abe K, Ono Y, Yoneyama H, et al., 2014; Ito D, Ishikawa C, Jeffery ND, Kitagawa M., 2021)
CFD	CSF fluid dynamic assessment	Better understanding the behavior of CSF flow dynamics. Potential diagnostic tool for CSF flow abnormalities.	In silico simulation, which is hard to represent the complexity of real-time CSF flow. Also, constrained by the MRI imaging modality that it uses to constrict its model.	No	(Kurtcuoglu V., 2011; Khani M, Sass LR, McCabe AR, et al., 2020; Linge SO, Mardal KA, Helgeland A, Heiss JD & Haughton V., 2014)

Note: Comparison of various competing imaging modalities in CSF fluid dynamic assessment

5. Conclusion

CSF plays a variety of vital roles, including cushioning the brain from trauma and clearing waste products via glymphatic clearance (Eklund A, Smielewski P, Chambers I, et al., 2007). Disruption in CSF flow and glymphatic clearance has been noted among those suffering from HCP, a common outcome of SAH. Under nonpathological conditions, CSF is secreted in a two-step process, the first being filtration of plasma as it flows from choroidal capillaries to the interstitium (Sakka L, Coll G, Chazal J., 2011). The second step involves the pumping of ions and bicarbonate with the subsequent entry of water (Owler BK, Pitham T & Wang D., 2010). CSF is mainly absorbed in the cranial arachnoid granulations; however, the absorptive process is influenced by changes in SAS pressure (Davson H, Hollingsworth G & Segal MB., 1970).

CSF flow has previously been characterized as projecting down through the spinal cord or up over the cerebral convexities (Bradley WG., 2015), although this is certainly a simplified view. The role the cardiovascular system plays in CSF

pulsations, as well as the interaction of CSF with anatomical structures like nerve roots and arachnoid trabeculae, certainly complicate this widespread understanding of the CSF flow pathway. Attempts to accurately predict and describe CSF flow include one, two, and three-dimensional models; however, even the most sophisticated models are limited by their computational and mathematical complexity. More recent models, which take into account "rest-of-body" compartments, are proving to be more useful when studying the effect of pathological conditions, such as hemorrhages, on CSF dynamics (Lakin WD, Stevens SA, Tranmer BI & Penar PL., 2003).

Pathological conditions like SAH significantly impact CSF flow. In several SAH-induced animal models, it has been shown that CSF is unable to flow into the basal cistern and paravascular spaces (Siler DA, Gonzalez JA, Wang RK, Cetas JS & Alkayed NJ., 2014), subject to backflow due to coagulation cascade products (Siler DA, Gonzalez JA, Wang RK, Cetas JS & Alkayed NJ., 2014), and restricted beyond the brain's basal regions (Golanov EV, Bovshik EI, Wong KK, et al., 2018; Gaberel T, Gakuba C, Goulay R, et al., 2014; Wang KC, Tang SC, Lee JE, et al., 2018). Scar tissue formation, increased red blood cells, and increased proteins commonly seen with SAH may result in increased viscosity, decreased vessel diameter, and thus increased vessel resistance; however, these effects may be limited to a local, and not global, level.

In addition to its direct impact on CSF flow, SAH may also induce noncommunicating (obstructive) or communicating (nonobstructive) HCP. With noncommunicating HCP, there is a lack of communication between ventricles (Greitz D, Greitz T & Hindmarsh T., 1997). In contrast, in communicating HCP, there is no block in the flow of CSF within the ventricular system (Koleva M & De Jesus O., 2022). A particular subtype of communicating HCP includes normal pressure HCP, which is characterized by normal ICP but impaired CSF circulation.

To effectively capture the dynamics of CSF flow in both normal and pathological conditions, many advanced imaging modalities have come forward. Those of note include PC-MRI, Time-SLIP, and mathematical analysis conducted by the CFD model, which relies on PC-MRI-generated data. PC-MRI relies on phase shift data to determine proton, and thus CSF, speed and flow (Wymer DT, Patel KP, Burke WF & Bhatia VK., 2020). The limitations of PC-MRI are directly addressed by Time-SLIP, which can characterize complex CSF fluid dynamics at any given time via comparison of CSF versus background signals (Yamada S & Kelly E., 2016).

Presently, there is a need for improved CSF flow models and imaging modalities. Elaboration upon "rest-of-body" compartment models appears to be a promising area of study, if additional factors affecting CSF flow are accounted for, including arterial pulse waves, respiratory waves, posture, and jugular venous posture (Sakka L, Coll G & Chazal J., 2011). Future imaging modalities should seek to become more structured and patient-centered in nature to appropriately assess CSF flow disruption in disease, including SAH and HCP.

List of Abbreviations

CSF – Cerebrospinal Fluid

SAS – Subarachnoid Space

HCP – Hydrocephalus

SAH – Subarachnoid Hemorrhage

NPH – Normal Pressure Hydrocephalus

IVH – Intraventricular Hemorrhage

ICP – Intracranial Pressure

ANP – Atrial Natriuretic Peptide

AVP – Arginine Vasopressin

PC-MRI – Phase-Contrast Magnetic Resonance Imaging

Time-SLIP – Time-Spatial Spin Labeling Inversion Pulse

CFD – Computation Fluid Dynamics

Ethics Approval and Consent to Participate

Not applicable.

Consent for Publication

Not applicable.

Availability of Data and Materials

Not applicable.

Funding

None

Conflict of Interest

None declared.

Acknowledgements

None declared.

References

Ma Q, Schlegel F, Bachmann SB, et al. (2019). Lymphatic outflow of cerebrospinal fluid is reduced in glioma. *Sci Rep*. *9*(1), 14815. doi:10.1038/s41598-019-51373-9.

Andersson K, Manchester IR, Andersson N, Shiriaev A, Malm J, Eklund A. (2007). Assessment of cerebrospinal fluid outflow conductance using an adaptive observer--experimental and clinical evaluation. *Physiol Meas*. *28*(11), 1355-1368. doi:10.1088/0967-3334/28/11/003.

Jessen NA, Munk ASF, Lundgaard I, Nedergaard M. (2015). The Glymphatic System: A Beginner's Guide. *Neurochem Res*. *40*(12), 2583-2599. doi:10.1007/s11064-015-1581-6.

Louveau A, Smirnov I, Keyes TJ, et al. (2016). Correction: Corrigendum: Structural and functional features of central nervous system lymphatic vessels. *Nature*, *533*(7602), 278-278. doi:10.1038/nature16999.

Eklund A, Smielewski P, Chambers I, et al. (2007). Assessment of cerebrospinal fluid outflow resistance. *Med Biol Eng Comput*. *45*(8), 719-735. doi:10.1007/s11517-007-0199-5.

Kaur J, Fahmy LM, Davoodi-Bojd E, et al. (2021). Waste Clearance in the Brain. *Front Neuroanat*, *15*, 665803. doi:10.3389/fnana.2021.665803.

Daversin-Catty C, Vinje V, Mardal KA, Rognes ME. (2020). The mechanisms behind perivascular fluid flow. *PLoS One*, *15*(12), e0244442. doi:10.1371/journal.pone.0244442.

Feigin VL, Lawes CM, Bennett DA, Barker-Collo SL, Parag V. (2009). Worldwide stroke incidence and early case fatality reported in 56 population-based studies: a systematic review. *The Lancet Neurology*, *8*(4), 355-369. doi:10.1016/S1474-4422(09)70025-0.

Kundra S, Mahendru V, Gupta V, Choudhary A. (2014). Principles of neuroanesthesia in aneurysmal subarachnoid hemorrhage. *J Anaesthesiol Clin Pharmacol*. *30*(3), 328. doi:10.4103/0970-9185.137261.

Petridis AK, Kamp MA, Cornelius JF, et al. (2017, March 31). Aneurysmal Subarachnoid Hemorrhage. *Deutsches Ärzteblatt international*. Published online March 31, 2017. doi:10.3238/arztebl.2017.0226.

Feigin VL, Rinkel GJE, Lawes CMM, et al. (2005). Risk Factors for Subarachnoid Hemorrhage: An Updated Systematic Review of Epidemiological Studies. *Stroke*, *36*(12), 2773-2780. doi:10.1161/01.STR.0000190838.02954.e8.

Kwon JH, Sung SK, Song YJ, Choi HJ, Huh JT, Kim HD. (2008). Predisposing Factors Related to Shunt-Dependent Chronic Hydrocephalus after Aneurysmal Subarachnoid Hemorrhage. *J Korean Neurosurg Soc*. *43*(4), 177. doi:10.3340/jkns.2008.43.4.177.

Hartman A. (2009). Normal Anatomy of the Cerebrospinal Fluid Compartment. In: *Cerebrospinal Fluid in Clinical Practice*. Elsevier; 5-10. doi:10.1016/B978-141602908-3.50005-4.

Bhattacharjee S, Rakesh D, Ramnadha R, Manas P. (2021). Subarachnoid Hemorrhage and Hydrocephalus. *Neurol India*. *69*(8), 429. doi:10.4103/0028-3886.332266.

M Das J, Biagioni MC. (2022). Normal Pressure Hydrocephalus. In: *StatPearls*. StatPearls Publishing; 2022. Accessed November 28, 2022. http://www.ncbi.nlm.nih.gov/books/NBK542247/.

Brust JCM. (2019). *Current Diagnosis & Treatment in Neurology*. 3rd edition. McGraw-Hill Medical.

Koleva M, De Jesus O. (2022). Hydrocephalus. In: *StatPearls*. StatPearls Publishing. Accessed November 27, 2022. http://www.ncbi.nlm.nih.gov/books/NBK560875/.

Chen S, Luo J, Reis C, Manaenko A, Zhang J. (2017). Hydrocephalus after Subarachnoid Hemorrhage: Pathophysiology, Diagnosis, and Treatment. *BioMed Research International*. *2017*, 1-8. doi:10.1155/2017/8584753.

Fang Y, Huang L, Wang X, et al. (2022). A new perspective on cerebrospinal fluid dynamics

after subarachnoid hemorrhage: From normal physiology to pathophysiological changes. *J Cereb Blood Flow Metab*. *42*(4), 543-558. doi:10.1177/0271678X211045748.

Galli F, Pandolfi M, Liguori A, Gurgitano M, Sberna M. (2021, January 24). Bleeding of Perivascular Spaces in Midbrain of a Young Patient with Head Trauma. *Cureus*. Published online, 2021. doi:10.7759/cureus.12884.

Quintin S, Barpujari A, Mehkri Y, Hernandez J, Lucke-Wold B. (2022, June 21). The glymphatic system and subarachnoid hemorrhage: disruption and recovery. *Explor Neuroprot Ther*. Published online June 21, 2022, 118-130. doi:10.37349/ent.2022.00023.

Li L, Ding G, Zhang L, et al. (2022). Aging-Related Alterations of Glymphatic Transport in Rat: In vivo Magnetic Resonance Imaging and Kinetic Study. *Front Aging Neurosci*. *14*, 841798. doi:10.3389/fnagi.2022.841798.

Papaioannou V, Czosnyka Z, Czosnyka M. (2022). Hydrocephalus and the neuro-intensivist: CSF hydrodynamics at the bedside. *ICMx*. *10*(1), 20. doi:10.1186/s40635-022-00452-9.

Whedon JM, Glassey D. (2009). Cerebrospinal fluid stasis and its clinical significance. *Altern Ther Health Med*. *15*(3), 54-60.

Sakka L, Coll G, Chazal J. (2011). Anatomy and physiology of cerebrospinal fluid. *European Annals of Otorhinolaryngology, Head and Neck Diseases*. *128*(6), 309-316. doi:10.1016/j.anorl.2011.03.002.

Speake T, Whitwell C, Kajita H, Majid A, Brown PD. (2001). Mechanisms of CSF secretion by the choroid plexus. *Microsc Res Tech*. *52*(1), 49-59. doi:10.1002/1097-0029(20010101)52:1<49::AID-JEMT7>3.0.CO;2-C.

Maria João Manzano. (2004). The system of cerebrospinal fluid-contacting neurons. Its supposed role in the nonsynaptic signal transmission of the brain. *Histology and Histopathology*. (19), 607-628. doi:10.14670/HH-19.607.

Brinker T, Stopa E, Morrison J, Klinge P. (2014). A new look at cerebrospinal fluid circulation. *Fluids Barriers CNS*. *11*(1), 10. doi:10.1186/2045-8118-11-10.

Owler BK, Pitham T, Wang D. (2010). Aquaporins: relevance to cerebrospinal fluid physiology and therapeutic potential in hydrocephalus. *Fluids Barriers CNS*. *7*(1), 15. doi:10.1186/1743-8454-7-15.

Damkier HH, Brown PD, Praetorius J. (2013). Cerebrospinal Fluid Secretion by the Choroid Plexus. *Physiological Reviews*, *93*(4), 1847-1892. doi:10.1152/physrev.00004.2013.

Gregoriades JMC, Madaris A, Alvarez FJ, Alvarez-Leefmans FJ. (2019). Genetic and pharmacological inactivation of apical Na^+-K^+-$2Cl^-$ cotransporter 1 in choroid plexus epithelial cells reveals the physiological function of the cotransporter. *American Journal of Physiology-Cell Physiology*, *316*(4), C525-C544. doi:10.1152/ajpcell.00026.2018.

Khasawneh A, Garling R, Harris C. (2018). Cerebrospinal fluid circulation: What do we know and how do we know it? *Brain Circ*. *4*(1), 14. doi:10.4103/bc.BC_3_18.

Faraci FM, Mayhan WG, Heistad DD. (1990). Effect of vasopressin on production of cerebrospinal fluid: possible role of vasopressin (V1)-receptors. *American Journal of Physiology-Regulatory, Integrative and Comparative Physiology*, *258*(1), R94-R98. doi:10.1152/ajpregu.1990.258.1.R94.

Kartalcı Ş, Erbay MF, Kahraman A, Çandır F, Erbay LG. (2021). Evaluation of CSF flow dynamics in patients with schizophrenia using phase-contrast cine MRI. *Psychiatry Research*, *304*, 114172. doi:10.1016/j.psychres.2021.114172.

Spector R, Robert Snodgrass S, Johanson CE. (2015). A balanced view of the cerebrospinal fluid composition and functions: Focus on adult humans. *Experimental Neurology*. *273*, 57-68. doi:10.1016/j.expneurol.2015.07.027.

Welch K, Friedman V. (1960). The Cerebrospinal Fluid Valves. *Brain*, *83*(3), 454-469. doi:10.1093/brain/83.3.454.

Pollay M. (2010). The function and structure of the cerebrospinal fluid outflow system. *Fluids Barriers CNS*. *7*(1), 9. doi:10.1186/1743-8454-7-9.

Davson H, Hollingsworth G, Segal MB. (1970). The Mechanism of Drainage of the

Cerebrospinal Fluid. *Brain*, *93*(4), 665-678. doi:10.1093/brain/93.4.665.

Bradley WG. (2015). CSF Flow in the Brain in the Context of Normal Pressure Hydrocephalus. *AJNR Am J Neuroradiol*. *36*(5), 831-838. doi:10.3174/ajnr.A4124.

Iliff JJ, Lee H, Yu M, et al. (2013). Brain-wide pathway for waste clearance captured by contrast-enhanced MRI. *J Clin Invest*. *123*(3), 1299-1309. doi:10.1172/JCI67677.

Donatelli D, Romagnoli L. (2020). Nonreflecting Boundary Conditions for a CSF Model of Fourth Ventricle: Spinal SAS Dynamics. *Bull Math Biol*. *82*(6), 77. doi:10.1007/s11538-020-00749-4.

Martin BA, Reymond P, Novy J, Balédent O, Stergiopulos N. (2012). A coupled hydrodynamic model of the cardiovascular and cerebrospinal fluid system. *American Journal of Physiology-Heart and Circulatory Physiology*, *302*(7), H1492-H1509. doi:10.1152/ajpheart.00658.2011.

Cirovic S, Kim M. (2012). A one-dimensional model of the spinal cerebrospinal-fluid compartment. *J Biomech Eng*. *134*(2), 021005. doi:10.1115/1.4005853.

Bertram CD, Brodbelt AR, Stoodley MA. (2005). The Origins of Syringomyelia: Numerical Models of Fluid/Structure Interactions in the Spinal Cord. *Journal of Biomechanical Engineering*, *127*(7), 1099-1109. doi:10.1115/1.2073607.

Clarke EC, Fletcher DF, Stoodley MA, Bilston LE. (2013). Computational fluid dynamics modelling of cerebrospinal fluid pressure in Chiari malformation and syringomyelia. *Journal of Biomechanics*, *46*(11), 1801-1809. doi:10.1016/j.jbiomech.2013.05.013.

Formaggia L, Gerbeau JF, Nobile F, Quarteroni A. (2001). On the coupling of 3D and 1D Navier–Stokes equations for flow problems in compliant vessels. *Computer Methods in Applied Mechanics and Engineering*, *191*(6-7), 561-582. doi:10.1016/S0045-7825(01)00302-4.

Del Bigio MR. (2001). Pathophysiologic Consequences of Hydrocephalus. *Neurosurgery Clinics of North America*. *12*(4), 639-649. doi:10.1016/S1042-3680(18)30022-6.

Van De Vyver AJ, Walz AC, Heins MS, et al. (2022). Investigating brain uptake of a non-targeting monoclonal antibody after intravenous and intracerebroventricular administration. *Front Pharmacol*. *13*, 958543. doi:10.3389/fphar.2022.958543.

Lakin WD, Stevens SA, Tranmer BI, Penar PL. (2003). A whole-body mathematical model for intracranial pressure dynamics. *J Math Biol*. *46*(4), 347-383. doi:10.1007/s00285-002-0177-3.

Loftspring MC, Wurster WL, Pyne-Geithman GJ, Clark JF. (2007). An in vitro model of aneurysmal subarachnoid hemorrhage: oxidation of unconjugated bilirubin by cytochrome oxidase. *J Neurochem*. *102*(6), 1990-1995. doi:10.1111/j.1471-4159.2007.04667.x.

Zhou J, Guo P, Guo Z, Sun X, Chen Y, Feng H. (2022). Fluid metabolic pathways after subarachnoid hemorrhage. *Journal of Neurochemistry*, *160*(1), 13-33. doi:10.1111/jnc.15458.

Wang HB, Wu QJ, Zhao SJ, et al. (2020). Early High Cerebrospinal Fluid Glutamate: A Potential Predictor for Delayed Cerebral Ischemia after Aneurysmal Subarachnoid Hemorrhage. *ACS Omega*. *5*(25), 15385-15389. doi:10.1021/acsomega.0c01472.

Siler DA, Gonzalez JA, Wang RK, Cetas JS, Alkayed NJ. (2014). Intracisternal Administration of Tissue Plasminogen Activator Improves Cerebrospinal Fluid Flow and Cortical Perfusion After Subarachnoid Hemorrhage in Mice. *Transl Stroke Res*. *5*(2), 227-237. doi:10.1007/s12975-014-0329-y.

Golanov EV, Bovshik EI, Wong KK, et al. (2018). Subarachnoid hemorrhage - Induced block of cerebrospinal fluid flow: Role of brain coagulation factor III (tissue factor). *J Cereb Blood Flow Metab*. *38*(5), 793-808. doi:10.1177/0271678X17701157.

Gaberel T, Gakuba C, Goulay R, et al. (2014). Impaired glymphatic perfusion after strokes revealed by contrast-enhanced MRI: a new target for fibrinolysis? *Stroke*, *45*(10), 3092-3096. doi:10.1161/STROKEAHA.114.006617.

Wang KC, Tang SC, Lee JE, et al. (2018). Impaired

microcirculation after subarachnoid hemorrhage in an in vivo animal model. *Sci Rep*. *8*(1), 13315. doi:10.1038/s41598-018-31709-7.

Goulay R, Flament J, Gauberti M, et al. (2017). Subarachnoid Hemorrhage Severely Impairs Brain Parenchymal Cerebrospinal Fluid Circulation in Nonhuman Primate. *Stroke*. *48*(8), 2301-2305. doi:10.1161/STROKEAHA.117.017014.

Plog BA, Nedergaard M. (2018). The Glymphatic System in Central Nervous System Health and Disease: Past, Present, and Future. *Annu Rev Pathol*. 13, 379-394. doi:10.1146/annurev-pathol-051217-111018.

Kertzscher U, Schneider T, Goubergrits L, Affeld K, Hänggi D, Spuler A. (2012). In vitro study of cerebrospinal fluid dynamics in a shaken basal cistern after experimental subarachnoid hemorrhage. *PLoS One*. *7*(8), e41677. doi:10.1371/journal.pone.0041677.

Kazumata K, Kamiyama H, Ishikawa T, et al. (2006). Clinical study of cerebrospinal fluid dynamics using 111In-DTPA SPECT in patients with subarachnoid hemorrhage. *Neurol Med Chir (Tokyo)*. *46*(1), 11-17; discussion 17-18. doi:10.2176/nmc.46.11.

Kosteljanetz M. (1984). CSF dynamics in patients with subarachnoid and/or intraventricular hemorrhage. *J Neurosurg*. *60*(5), 940-946. doi:10.3171/jns.1984.60.5.0940.

Ursino M, Lodi CA. (1997). A simple mathematical model of the interaction between intracranial pressure and cerebral hemodynamics. *J Appl Physiol*. *82*(4), 1256-1269. doi:10.1152/jappl.1997.82.4.1256.

Shinya Yamada, (2021). Cerebrospinal fluid dynamics. *Croat Med J*. *62*(4), 399-410. doi:10.3325/cmj.2021.62.399.

Jacobson EE, Fletcher DF, Morgan MK, Johnston IH. (1999). Computer modelling of the cerebrospinal fluid flow dynamics of aqueduct stenosis. *Med Biol Eng Comput*. *37*(1), 59-63. doi:10.1007/BF02513267.

Bloomfield IG, Johnston IH, Bilston LE. (1998). Effects of Proteins, Blood Cells and Glucose on the Viscosity of Cerebrospinal Fluid. *Pediatr Neurosurg*. *28*(5), 246-251. doi:10.1159/000028659.

Lindstrøm EK, Ringstad G, Sorteberg A, Sorteberg W, Mardal KA, Eide PK. (2019). Magnitude and direction of aqueductal cerebrospinal fluid flow: large variations in patients with intracranial aneurysms with or without a previous subarachnoid hemorrhage. *Acta Neurochir (Wien)*. *161*(2), 247-256. doi:10.1007/s00701-018-3730-6.

Abolfazli E, Fatouraee N, Seddighi AS. (2016). Effects of lumbar drainage on CSF dynamics in subarachnoid hemorrhage condition: A computational study. *Comput Biol Med*. 77, 49-58. doi:10.1016/j.compbiomed.2016.08.003.

Khani M, Sass LR, Sharp MK, et al. (2020). In vitro and numerical simulation of blood removal from cerebrospinal fluid: comparison of lumbar drain to Neurapheresis therapy. *Fluids Barriers CNS*, *17*(1), 23. doi:10.1186/s12987-020-00185-5.

Li X. (2021). Subject-Specific Head Model Generation by Mesh Morphing: A Personalization Framework and Its Applications. *Front Bioeng Biotechnol*. 9, 706566. doi:10.3389/fbioe.2021.706566.

Wittek A, Joldes G, Couton M, Warfield SK, Miller K. (2010). Patient-specific non-linear finite element modelling for predicting soft organ deformation in real-time; Application to non-rigid neuroimage registration. *Progress in Biophysics and Molecular Biology*. *103*(2-3), 292-303. doi:10.1016/j.pbiomolbio.2010.09.001.

Lefever JA, Jaime García J, Smith JH. (2013). A patient-specific, finite element model for noncommunicating hydrocephalus capable of large deformation. *Journal of Biomechanics*. *46*(8), 1447-1453. doi:10.1016/j.jbiomech.2013.03.008.

Vardakis JC, Tully BJ, Ventikos Y. (2013). Exploring the efficacy of endoscopic ventriculostomy for hydrocephalus treatment via a multicompartmental poroelastic model of CSF transport: a computational perspective. *PLoS One*, *8*(12), e84577. doi:10.1371/journal.pone.0084577.

Gholampour S, Fatouraee N. (2021). Boundary conditions investigation to improve computer simulation of cerebrospinal fluid dynamics in

hydrocephalus patients. *Commun Biol*. *4*(1), 394. doi:10.1038/s42003-021-01920-w

Balestrazzi P, de Gressi S, Donadio A, Lenzini S. (1989). Periaqueductal gliosis causing hydrocephalus in a patient with neurofibromatosis type 1. *Neurofibromatosis*. *2*(5-6), 322-325.

Greitz D, Greitz T, Hindmarsh T. (1997). A new view on the CSF-circulation with the potential for pharmacological treatment of childhood hydrocephalus. *Acta Paediatr*. *86*(2), 125-132. doi:10.1111/j.1651-2227.1997.tb08850.x.

Sokal P, Birski M, Rusinek M, Paczkowski D, Zieliński P, Harat A. (2012). Endoscopic third ventriculostomy in treatment of hydrocephalus. *Wiitm*. *4*, 280-285. doi:10.5114/wiitm.2011.30810.

Farb R, Rovira À. (2020). Hydrocephalus and CSF Disorders. In: Hodler J, Kubik-Huch RA, von Schulthess GK, eds. *Diseases of the Brain, Head and Neck, Spine 2020–2023*. IDKD Springer Series. Springer International Publishing; 11-24. doi:10.1007/978-3-030-38490-6_2.

Maller VV, Gray RI. (2016). Noncommunicating Hydrocephalus. *Seminars in Ultrasound, CT and MRI*, *37*(2), 109-119. doi:10.1053/j.sult.2015.12.004.

Linninger AA, Sweetman B, Penn R. (2009). Normal and hydrocephalic brain dynamics: the role of reduced cerebrospinal fluid reabsorption in ventricular enlargement. *Ann Biomed Eng*. *37*(7), 1434-1447. doi:10.1007/s10439-009-9691-4.

Krauss JK, Regel JP, Vach W, Droste DW, Borremans JJ, Mergner T. (1996). Vascular Risk Factors and Arteriosclerotic Disease in Idiopathic Normal-Pressure Hydrocephalus of the Elderly. *Stroke*, *27*(1), 24-29. doi:10.1161/01.STR.27.1.24.

Tang Y min, Yao Y, Xu S, et al. (2021). White Matter Microstructural Damage Associated with Gait Abnormalities in Idiopathic Normal Pressure Hydrocephalus. *Front Aging Neurosci*. *13*, 660621. doi:10.3389/fnagi.2021.660621.

Vivas-Buitrago T, Lokossou A, Jusué-Torres I, et al. (2019). Aqueductal Cerebrospinal Fluid Stroke Volume Flow in a Rodent Model of Chronic Communicating Hydrocephalus: Establishing a Homogeneous Study Population for Cerebrospinal Fluid Dynamics Exploration. *World Neurosurg*. *128*, e1118-e1125. doi:10.1016/j.wneu.2019.05.093.

Korbecki A, Zimny A, Podgórski P, Sąsiadek M, Bladowska J. (2019). Imaging of cerebrospinal fluid flow: fundamentals, techniques, and clinical applications of phase-contrast magnetic resonance imaging. *pjr*. *84*, 240-250. doi:10.5114/pjr.2019.86881.

Yamada S, Kelly E. (2016). Cerebrospinal Fluid Dynamics and the Pathophysiology of Hydrocephalus: New Concepts. *Semin Ultrasound CT MR*. *37*(2), 84-91. doi:10.1053/j.sult.2016.01.001.

Wymer DT, Patel KP, Burke WF, Bhatia VK. (2020). Phase-Contrast MRI: Physics, Techniques, and Clinical Applications. *RadioGraphics*. *40*(1), 122-140. doi:10.1148/rg.2020190039.

Nitz WR, Bradley WG, Watanabe AS, et al. (1992). Flow dynamics of cerebrospinal fluid: assessment with phase-contrast velocity MR imaging performed with retrospective cardiac gating. *Radiology*, *183*(2), 395-405. doi:10.1148/radiology.183.2.1561340.

Yamada S, Tsuchiya K, Bradley WG, et al. (2015). Current and Emerging MR Imaging Techniques for the Diagnosis and Management of CSF Flow Disorders: A Review of Phase-Contrast and Time–Spatial Labeling Inversion Pulse. *AJNR Am J Neuroradiol*. *36*(4), 623-630. doi:10.3174/ajnr.A4030.

Fillingham P, Rane Levendovszky S, Andre J, et al. (2022). Patient-specific computational fluid dynamic simulation of cerebrospinal fluid flow in the intracranial space. *Brain Research*, *1790*, 147962. doi:10.1016/j.brainres.2022.147962.

Kurtcuoglu V. (2011). Computational Fluid Dynamics for the Assessment of Cerebrospinal Fluid Flow and Its Coupling with Cerebral Blood Flow. In: Miller K, ed. *Biomechanics of the Brain*. Biological and Medical Physics, Biomedical Engineering. Springer New York; 169-188. doi:10.1007/978-1-4419-9997-9_8.

Battal B, Kocaoglu M, Bulakbasi N, Husmen G,

Tuba Sanal H, Tayfun C. (2011). Cerebrospinal fluid flow imaging by using phase-contrast MR technique. *BJR*. *84*(1004), 758-765. doi:10.1259/bjr/66206791.

Barkhof F, Kouwenhoven M, Scheltens P, Sprenger M, Algra P, Valk J. (1994). Phase-contrast cine MR imaging of normal aqueductal CSF flow. Effect of aging and relation to CSF void on modulus MR. *Acta Radiol*, *35*(2), 123-130.

Lee JH, Lee HK, Kim JK, Kim HJ, Park JK, Choi CG. (2004). CSF Flow Quantification of the Cerebral Aqueduct in Normal Volunteers Using Phase Contrast Cine MR Imaging. *Korean J Radiol*, *5*(2), 81. doi:10.3348/kjr.2004.5.2.81.

Sharma AK, Gaikwad S, Gupta V, Garg A, Mishra NK. (2008). Measurement of peak CSF flow velocity at cerebral aqueduct, before and after lumbar CSF drainage, by use of phase-contrast MRI: Utility in the management of idiopathic normal pressure hydrocephalus. *Clinical Neurology and Neurosurgery*, *110*(4), 363-368. doi:10.1016/j.clineuro.2007.12.021.

Alperin N, Vikingstad EM, Gomez-Anson B, Levin DN. (1996). Hemodynamically independent analysis of cerebrospinal fluid and brain motion observed with dynamic phase contrast MRI. *Magn Reson Med*. *35*(5), 741-754. doi:10.1002/mrm.1910350516.

Ohtonari T, Nishihara N, Ota S, Tanaka A. (2018). Novel Assessment of Cerebrospinal Fluid Dynamics by Time-Spatial Labeling Inversion Pulse Magnetic Resonance Imaging in Patients with Chiari Malformation Type I. *World Neurosurgery*, *112*, e165-e171. doi:10.1016/j.wneu.2018.01.001.

Shibukawa S, Miyati T, Niwa T, et al. (2018). Time-spatial Labeling Inversion Pulse (Time-SLIP) with Pencil Beam Pulse: A Selective Labeling Technique for Observing Cerebrospinal Fluid Flow Dynamics. *MRMS*, *17*(3), 259-264. doi:10.2463/mrms.tn.2017-0032.

Takeuchi K, Ono A, Hashiguchi Y, et al. (2017). Visualization of cerebrospinal fluid flow in syringomyelia through noninvasive magnetic resonance imaging with a time-spatial labeling inversion pulse (Time-SLIP). *The Journal of Spinal Cord Medicine*, *40*(3), 368-371. doi:10.1080/10790268.2016.1140391.

Abe K, Ono Y, Yoneyama H, et al. (2014). Assessment of Cerebrospinal Fluid Flow Patterns Using the Time-Spatial Labeling Inversion Pulse Technique with 3T MRI: Early Clinical Experiences. *Neuroradiol J*. *27*(3), 268-279. doi:10.15274/NRJ-2014-10045.

Ito D, Ishikawa C, Jeffery ND, Kitagawa M. (2021). Cerebrospinal fluid flow on time-spatial labeling inversion pulse images before and after treatment of congenital hydrocephalus in a dog. *J Vet Intern Med*. *35*(1), 490-496. doi:10.1111/jvim.16020.

Khani M, Sass LR, McCabe AR, et al. (2020). Impact of Neurapheresis System on Intrathecal Cerebrospinal Fluid Dynamics: A Computational Fluid Dynamics Study. *J Biomech Eng*. *142*(2), 0210061-0210069. doi:10.1115/1.4044308.

Linge SO, Mardal KA, Helgeland A, Heiss JD, Haughton V. (2014). Effect of craniovertebral decompression on CSF dynamics in Chiari malformation type I studied with computational fluid dynamics: Laboratory investigation. *J Neurosurg Spine*. *21*(4), 559-564. doi:10.3171/2014.6.SPINE13950.